Applied Numerical Mathematics 147 (2020) 19–30

Contents lists available at ScienceDirect

Applied Numerical Mathematics

www.elsevier.com/locate/apnum

The method of regularized successive iterations for coupled physics conductivity imaging from a single internal data

A. Tamasan [a], A. Timonov [b,c,*]

[a] Department of Mathematics, University of Central Florida, Orlando, FL, USA
[b] Division of Mathematics and Computer Science, University of South Carolina Upstate, Spartanburg, SC, USA
[c] The Steklov Institute of Mathematics (S. Petersburg branch), S. Petersburg, Russia

ARTICLE INFO

Article history:
Received 27 April 2019
Received in revised form 4 July 2019
Accepted 8 August 2019
Available online 13 August 2019

Keywords:
Coupled physics conductivity imaging
Inverse conductivity problem
Weighted least gradient problem
Regularization
Numerical experiments

ABSTRACT

We consider the numerical solution of an inverse conductivity problem that arises in coupled physics conductivity imaging. We propose and develop the method of regularized successive iterations based on a regularized weighted least gradient Robin problem. Unlike the existing numerical techniques, the main novelty is that recovering the electrical conductivity from a single internal data does not require the boundary data. The performance of the proposed method is demonstrated by computer simulations of coupled physics conductivity imaging.

1. Introduction

We consider the numerical solution of the problem of recovering the electrical conductivity σ in a bounded domain $\Omega \subset R^d, d = 2, 3$ filled with the conductive medium from the magnitude of current density field in Ω. This problem arises in coupled physics conductivity imaging (see, e.g., [15,22] for detail).

Suppose the boundary $\partial\Omega$ of Ω is Lipschitz, and the conductivity σ is isotropic and positive. For simplicity, we assume that two identical electrodes $e_\pm$ are placed on the boundary, so that $e_\pm \subset \partial\Omega$ are two connected subsets with the mutually disjoint closures, $|e_+| = |e_-| = |e|$, and the electrodes have the same effective electrode impedance $z_+ = z_- = z > 0$. The direct currents $I_\pm$ are injected into and ejected from Ω through the electrode electrical circuit. Because of no electrical charges in a conductive medium, $I_- = I_+ = I$, and the voltage potential u satisfies the Robin problem

$$\nabla \cdot (\sigma(x)\nabla u) = 0 \text{ in } \Omega, \tag{1}$$

subject to

$$\sigma(\nabla u \cdot \nu) + \varphi u = f \text{ on } \partial\Omega, \tag{2}$$

where ν denotes the outer unit normal to the boundary, and

$$\varphi(x) = \begin{cases} 1/z, x \in e_\pm, \\ \beta/z, x \in \partial\Omega \setminus e_\pm, \end{cases} \quad \text{and} \quad f(x) = \begin{cases} (R_e/z) \pm I, x \in e_\pm, \\ 0, x \in \partial\Omega \setminus e_\pm. \end{cases} \tag{3}$$

* Corresponding author.
E-mail addresses: tamasan@math.ucf.edu (A. Tamasan), atiomonov@uscupstate.edu, altim@pdmi.ras.ru (A. Timonov).

https://doi.org/10.1016/j.apnum.2019.08.006
0168-9274/

The constant $R_e > 0$ accounts for the effective electrode resistance, and $0 < \beta \ll 1$ is a small number, such that z/β accounts for the very large boundary electrical impedance outside the electrodes. Note that the need to introduce the number β is due to a sufficient condition of uniqueness of the solution (see Section 2 and also Theorem 1b in [23]). It is well known that the forward problem (1), (2) has a unique solution in $H^1(\Omega)$.

Exploiting the Ohm's law and introducing the internal data $a = \sigma|\nabla u|$, one could formally transform the equation (1) to a weighted 1-Laplacian with the weight function a and formulate a coupled physics inverse conductivity problem in terms of finding a solution to this equation given a single internal data a. Once its solution u is found, the conductivity may be reconstructed as $\sigma = a/|\nabla u|$ at least for the regions where the gradient ∇u is not vanished. This attempt was first made in [5]. However, such an inverse problem is ill-posed in the sense of Hadamard, and some nonexistence and non-uniqueness examples were demonstrated in [5] in the case of the Neumann boundary condition. Therefore, a reconstruction algorithm employing the magnitudes of two internal current densities was proposed in [5].

The reconstruction of conductivity using just one internal data a was originated with the fact that equipotential surfaces are minimal surfaces in a Riemannian space determined by this internal data [12]. Using the co-area formula (e.g., [27]), this fact further lead to the weighted least gradient formulation for the Dirichlet problem in [13] and [14]. Both the existence and uniqueness of such weighted gradient problems were studied in [4] and [10] and extended to the unique determination of the shape and position of the perfectly insulated and conducting inclusions in [9,10]. In this paper we present the method for quantitative imaging where the conductivity is bounded. Under some a priori assumptions, a structural stability result for a weighted least gradient problem can be found in [17]. When the entire current density field is available inside the stability results were established in [7] for the unperturbed Dirichlet data and in [8] for the partial data. The existing numerical reconstruction methods using knowledge of one current density field are based either on the level set methods [6], [12] and [24] or on the variational approach to the weighted least gradient Dirichlet problems [10], [13]. However, current practices of acquiring the internal data requires two rotations made by a MRI system [20], yielding any additional measurements of the boundary voltage potential impractical.

Motivated by the challenge to completely eliminate the boundary data, in [16] the coupled physics inverse conductivity problem was studied within the framework of the Complete Electrode Model [21]. However, the characterization of the non-uniqueness result given in [16] allows for reducing only a part, though essential, of boundary data that is needed to ensure the uniqueness result. This motivates us to introduce the Robin model (1)–(3) for use in the coupled physics inverse conductivity problem. But even within the framework of this model, the issues of uniqueness and stability still remain ambiguous. Indeed, if $\beta = 0$ in (3), then for any $\psi : Range(u) \to Range(u)$ an increasing Lipschitz continuous function, satisfying $\psi(t) = t$ for $t \in u(e_+) \cup u(e_-)$, one can verify that $u_\psi = \psi \circ u$ is another solution of the Robin problem corresponding to the conductivity $\sigma/(\psi' \circ u)$, while the magnitude of the current density field does not change. It follows from [23] that for $\beta > 0$, the conductivity σ is uniquely determined by the unperturbed internal data a. However, in practice the internal data a is always perturbed due to the roundoff and truncation errors and measurement noise. Under these conditions, for the small values of $\beta > 0$ a matrix resulted from the finite-difference approximation of the Robin problem (1)–(3) is ill-conditioned. This implies numerical instability. To correct for the lack of numerical stability, we propose and develop the method of regularized successive iterations that allows for constructing some minimizing sequences for the regularized weighted least gradient Robin functional. Beginning from a certain number, the members of a minimizing sequence are used to approximate the solution (σ, u) of the coupled physics inverse conductivity problem.

In Section 2 we outline briefly some analytical results that are used in our paper. In Section 3 we introduce a regularized weighted least gradient Robin functional and briefly sketch a compactness property of minimizing sequences and the continuous dependence of the regularized problem on the data. The method of regularized successive iterations is described in Section 4. The model problem is introduced in Section 5 together with the description of computer simulations and some results of numerical experiments. The paper is concluded with some remarks in Section 6.

2. Preliminaries

Suppose

$$\sigma \in C^{1/2}(\overline{\Omega}) \text{ and } \sigma \in C^2(\partial\Omega),\ \sigma > 0. \tag{4}$$

As in [13] we apply the variational approach to the inverse Robin model and introduce the functional

$$G(v; a, \varphi, h) = \int_\Omega a|\nabla v| dx + \frac{1}{2}\int_{\partial\Omega} \varphi(v-h)^2 ds, \tag{5}$$

where $h = f/\varphi$ and $h = 0$ on, respectively off the electrodes.

Since $\beta > 0$, for sufficiently smooth coefficients in the Robin condition (2), the uniqueness result established in [23] can be restated as follows. Let $BV_2(\Omega)$ be the space of functions of bounded variation with square integrable trace on the boundary. The differential expression $|\nabla u| dx$ in the first term in (5) is understood as a Radon measure applied to the bounded continuous function a.

Theorem 1. *Suppose the function σ satisfies the condition (4), and the coefficients φ and f in (2) are chosen as in (3). Let $u \in H^1(\Omega)$ be the solution of the Robin problem (1)–(2). Then $a \in C^{1/2}(\overline{\Omega})$, and u is the unique minimizer of the functional $G(\cdot; a, \varphi, h)$ in $BV_2(\Omega)$, i.e.,*

$$u = argmin\{G(v; a, \varphi, h) : v \in BV_2(\Omega)\}. \tag{6}$$

Moreover, $u \in C^{1,1/2}(\overline{\Omega})$ and

$$\sigma = \frac{a}{|\nabla u|}. \tag{7}$$

This result allows us to elucidate the way of recovering the conductivity from the internal data, which consists in the construction of minimizing sequences for the functional (5). However, it is not clear how to construct directly a minimizing sequence. Therefore, we regularize the functional (5) that has the unique minimizer in $H^1(\Omega)$ for every $\alpha > 0$. The main difficulty is that the sequence of these minimizers may not be bounded in $H^1(\Omega)$, but, fortunately, it is bounded in $BV_2(\Omega)$. Then the Rellich-Kondrachov compactness theorem allows for convergence of a subsequence, and the uniqueness result above allows one to conclude convergence of the entire sequence (see Theorem 2).

3. Regularization

It follows from the classical arguments and [12,13,10] that under our hypothesis on the regularity of the coefficients, the internal data $a = \sigma|\nabla u| \in C^{1/2}(\overline{\Omega})$ and it is bounded away from zero, i.e.,

$$\inf a > 0. \tag{8}$$

Let $u_h \in H^1(\Omega)$ be the harmonic extension of h into Ω, i.e.,

$$\Delta u_h = 0 \text{ in } \Omega, \tag{9}$$

$$u_h = h \text{ on } \partial\Omega. \tag{10}$$

For an arbitrary fixed parameter $\alpha > 0$ we introduce the regularized functional

$$G^\alpha(v; a) = \int_\Omega a|\nabla v|dx + \frac{1}{2}\int_{\partial\Omega} \varphi(v-h)^2 ds + \frac{\alpha}{2}\int_\Omega |\nabla(v-u_h)|^2 dx. \tag{11}$$

For convenience, the explicit dependence on φ and h, which are fixed throughout the paper, is omitted. Note that if $\alpha = 0$, then we obtain the functional (5). The unique solvability of the variational problem

$$argmin\left\{G^\alpha(v; a) : v \in H^1(\Omega)\right\}$$

follows from the classical convex theory due to the weak lower semicontinuity of the first term in the functional (11) in $H^1(\Omega)$.

To establish the regularizing property of $G^\alpha(v; a)$, we make the following assumptions. Let $\{a_n\} \subset L^2(\Omega)$ be a sequence of positive functions, such that

$$\|a_n - a\|_{L_2(\Omega)} \to 0 \text{ as } n \to \infty, \tag{12}$$

and $\alpha_n \to 0$ be a decreasing sequence, such that

$$\lim_{n\to\infty} \frac{\|a - a_n\|_{L^2(\Omega)}}{\alpha_n} = 0. \tag{13}$$

For every n we denote u_n the unique minimizer of $G^{\alpha_n}(v; a_n)$, i.e.,

$$u_n = argmin\{G^{\alpha_n}(v; a_n) : v \in H^1(\Omega)\}. \tag{14}$$

The regularizing property of $G^\alpha(v; a)$ follows from Theorem 1 and compactness of the minimizing sequence $\{u_n\}$ established in [23]. For clarity,

Theorem 2. *Suppose $\Omega \subset R^d$, $d = 2, 3$ is a bounded Lipschitz domain with the connected boundary. Under the assumptions (8), (12) and (13), let $\{u_n\}$ be the sequence of minimizers in (14). Then the following convergence results hold*

$$G^{\alpha_n}(u_n; a_n) \to G(u; a) \text{ as } n \to \infty, \tag{15}$$

and for all $1 \le q < d/(d-1)$,

$$\|u_n - u\|_{L^q(\Omega)} \to 0, u \text{ as } n \to \infty. \tag{16}$$

Proof. We argue that the entire sequence is convergent. Indeed, it follows from [23] that the sequence $\{u_n\}$ is bounded in $W^{1,1}(\Omega)$ and by the Rellich-Kondrachov compactness embedding in $L^q(\Omega)$ it is compact. It was also shown in [23] that any limit point $u^* \in L^q(\Omega)$ of a convergent subsequence which has the bounded total variation, has a square integrable trace on $\partial\Omega$. Besides, it is a minimizer of the functional $G(\cdot;a)$ in $BV_2(\Omega)$. By the uniqueness result in Theorem 1, any such limit u^* must coincide with u. Hence, the entire sequence $\{u_n\}$ is convergent.

4. The method of regularized successive iterations

4.1. The α-parametric Robin problems

Recall that for the fixed coefficients φ and h and regularization parameter $\alpha > 0$ the regularized functional (11) depends on the internal data a only. By analogy let us introduce the functional

$$F^\alpha(u;\sigma) = \frac{1}{2}\left\{ \int_\Omega \sigma|\nabla v|^2 dx + \alpha \int_\Omega |\nabla(v-u_h)|^2 dx + \int_{\partial\Omega} \varphi(v-u_h)^2 ds \right\}. \tag{17}$$

We observe now that the functional $F^\alpha(u;\sigma)$ depends on the unknown conductivity σ. However, this functional possesses a key property for constructing the regularized successive iterations. Namely, using the identity

$$\int_\Omega \nabla u_h \cdot \nabla v dx = \int_{\partial\Omega} (\nabla u_h \cdot \nu) v ds,$$

it is easy to show that $F^\alpha(v;\sigma)$ is the energy functional for the α-parametric Robin problem

$$\nabla \cdot (\sigma + \alpha)\nabla u = 0 \text{ in } \Omega, \tag{18}$$

$$(\sigma + \alpha)(\nabla u \cdot \nu) + \varphi u = \alpha(\nabla u_h \cdot \nu) \text{ on } \partial\Omega. \tag{19}$$

Moreover, if $u_\alpha \in H^1(\Omega)$ is the solution to the problem (18)–(19), then

$$F^\alpha(u_\alpha : \sigma) \le F^\alpha(v : \sigma)\ \forall v \in H^1(\Omega). \tag{20}$$

The following result provides a theoretical justification for the method of regularized successive iterations using the α-parametric Robin problem instead of applying the existing methods for minimizing the functional $G^\alpha(v;a)$.

Theorem 3. *Suppose $a \in L^2(\Omega)$, $\varphi \in L^\infty(\Omega)$ are positive. Let $u_h \in H^1(\Omega)$ be the harmonic extension of $h \in H^{1/2}(\partial\Omega)$. Let $v \in H^1(\Omega)$ be such that $a/|\nabla v| \in L_\infty(\Omega)$, and let $u_\alpha \in H^1(\Omega)$ be the solution to the Robin problem*

$$\nabla \cdot \left(\frac{a}{|\nabla v|} + \alpha\right)\nabla u = 0 \text{ in } \Omega, \tag{21}$$

$$\left(\frac{a}{|\nabla v|} + \alpha\right)(\nabla u \cdot \nu) + \varphi u = \alpha(\nabla u_h \cdot \nu) \text{ on } \partial\Omega. \tag{22}$$

Then

$$G^\alpha(u_\alpha; a) \le G^\alpha(v; a), \tag{23}$$

and if the equality in (23) holds, then $u_\alpha = v$.

Proof. Since u_α is the global minimizer of $F^\alpha(v;\sigma)$ in $H^1(\Omega)$, we have

$$\begin{aligned} G^\alpha(v;a) &= \int_\Omega a|\nabla v| dx + \frac{\alpha}{2}\int_\Omega |\nabla(v-u_h)|^2 dx + \int_{\partial\Omega} \varphi(v-h)^2 ds, \\ &= \frac{1}{2}\int_\Omega a|\nabla v| dx + F^\alpha(v; \frac{a}{|\nabla v|}), \\ &\ge \frac{1}{2}\int_\Omega a|\nabla v| dx + F^\alpha(u_\alpha; \frac{a}{|\nabla v|}). \end{aligned} \tag{24}$$

Estimating the term

$$\int_\Omega a|\nabla u_\alpha|dx = \int_\Omega \left(\frac{a}{|\nabla v|}\right)^{1/2}|\nabla v|\cdot\left(\frac{a}{|\nabla v|}\right)^{1/2}|\nabla u_\alpha|dx$$
$$\leq \left(\int_\Omega \frac{a}{|\nabla v|}|\nabla v|^2 dx\right)^{1/2}\cdot\left(\int_\Omega \frac{a}{|\nabla v|}|\nabla u_\alpha|^2 dx\right)^{1/2}$$
$$\leq \frac{1}{2}\int_\Omega a|\nabla v|dx + \frac{1}{2}\int_\Omega \frac{a}{|\nabla v|}|\nabla u_\alpha|^2 dx,$$

we obtain

$$G^\alpha(u_\alpha;a) = \int_\Omega a|\nabla u_\alpha|dx + \frac{\alpha}{2}\int_\Omega |\nabla(u_\alpha - u_h)|^2 dx + \int_{\partial\Omega}\varphi(u_\alpha - h)^2 ds,$$
$$\leq \int_\Omega a|\nabla v|dx + F^\alpha\left(u_\alpha;\frac{a}{|\nabla v|}\right) \leq G^\alpha(v;a). \tag{25}$$

Then the estimate (23) follows from (24) and (25). If the equality holds in (23), then it also holds in (24). In particular,

$$F^\alpha\left(u_\alpha;\frac{a}{|\nabla v|}\right) = F^\alpha\left(v;\frac{a}{|\nabla v|}\right).$$

This means that v is also the global minimizer of $F^\alpha\left(v;\frac{a}{|\nabla v|}\right)$ in $H^1(\Omega)$. Because of uniqueness of the minimizer, $u_\alpha = v$.

4.2. Constructing the regularized successive iterations

Based on Theorems 1, 2, and 3 we propose a simple, but computationally efficient, iterative procedure for constructing a minimizing sequence for the functional $G^\alpha(v;a)$. Assume that an upper bound $\overline{\sigma}$ of conductivity is known *apriori*, and the harmonic extension u_h and its normal derivative $\psi = \nabla u_h\cdot\nu$ have been precomputed.

- **Initialization.** Given $a, \varphi, h, u_h, \psi, \overline{\sigma}$, and a decreasing sequence $\alpha_n \to 0^+$, and set $\sigma_0 \equiv 1$ in $\overline{\Omega}$.
- **Iteration 1.** Solve the problem

$$\nabla\cdot(\sigma_0+\alpha_1)\nabla u = 0 \text{ in } \Omega,$$
$$(\sigma_0+\alpha_1)(\nabla u\cdot\nu) + \varphi u = \alpha_1\psi \text{ on } \partial\Omega,$$

  and set u_0 equals its solution.
- **Iteration k.** Assume that the $(k-1)$s iteration was made in which the pair (σ_{k-1}, u_{k-1}) was computed. Then we update to

$$\sigma_k = \max\left(\frac{a}{|\nabla u_{k-1}|}, \overline{\sigma}\right\},$$

  and solve the problem

$$\nabla\cdot(\sigma_k+\alpha_{k+1})\nabla u = 0 \text{ in } \Omega,$$
$$(\sigma_k+\alpha_{k+1})(\nabla u\cdot\nu) + \varphi u = \alpha_{k+1}\psi \text{ on } \partial\Omega.$$

  Set u_k equals its solution.
  In each kth iteration check the stopping criteria

$$\max||\nabla u_k| - |\nabla u_{k-1}|| \leq \frac{\delta}{\overline{\sigma}}$$

  and

$$\frac{\|\sigma_k - \sigma_{k-1}\|_2}{\|\sigma_k\|_2} \leq TOL,$$

  where Δ is the prescribed level of the roundoff and truncation error and TOL is the tolerance level. If they are not satisfied, reassign the quantities for $k-1 := k$ and repeat **Iteration k**. Otherwise, set $\sigma^\alpha = \sigma_k$ and $u^\alpha = u_k$.

4.3. A difference scheme for the α-parametric Robin problem

To implement the method of regularized successive iterations, at each iteration for the fixed parameter α one needs to solve numerically the Robin problem (18)–(19). Clearly, the rate of convergence of the iterative procedure and accuracy of reconstruction depend strongly on how accurate this problem is solved numerically. To ensure the appropriate accuracy, we use the following difference scheme.

Since the harmonic extension u_h is precomputed, it is natural to represent the solution of the problem (18)–(19) in the form $u_\alpha = w + u_h$, where the function w satisfies the inhomogeneous Robin problem

$$\nabla \cdot (\sigma_\alpha \nabla w) = -\nabla \cdot (\sigma_\alpha \nabla u_h) \text{ in } \Omega, \tag{26}$$

$$\sigma_\alpha (\nabla w \cdot \nu) + \varphi w = f_h \text{ on } \partial\Omega, \tag{27}$$

where $\sigma_\alpha = \sigma + \alpha$, $f_h = -\sigma(\nabla u_h \cdot \nu) - \varphi u_h$. The physical interpretation is that in a conductive medium, the voltage potential u_h induces the current density field $J_h = -\hat{\sigma}\nabla u_h$, the divergence of which generates the secondary source distribution F_h in Ω in accordance with the Kirchhoff's law. This representation is advantageous also because the harmonic extension u_h can be computed with high-order accuracy.

Without loss of generality, we consider further the α-parametric Robin problem (26)–(19) in two dimensions. Suppose the closure of Ω is the unit square

$$\overline{\Omega} = \{(x_1, x_2) : 0 \le x_1 \le 1, 0 \le x_2 \le 1\}.$$

In this case, the problem (26)–(19) is written as

$$\sum_{m=1}^{2} \partial_{x_m} \left(\sigma_\alpha(x) \partial_{x_m} w\right) = -F_h(x) \text{ in } \Omega, \tag{28}$$

$$\sigma_\alpha \partial_{x_1} w = \frac{\varepsilon}{z} w - \gamma_{11} \text{ if } x_1 = 0, \tag{29}$$

$$\sigma_\alpha \partial_{x_2} w = \frac{1}{z} w - \gamma_{12} \text{ if } x_2 = 0, \tag{30}$$

$$-\sigma_\alpha \partial_{x_1} w = \frac{\varepsilon}{z} w - \gamma_{21} \text{ if } x_1 = 1, \tag{31}$$

$$-\sigma_\alpha \partial_{x_2} w = \frac{1}{z} w - \gamma_{22} \text{ if } x_2 = 1, \tag{32}$$

where $x = (x_1, x_2)$, $\sigma_\alpha = \sigma + \alpha$, $F_h = \nabla \cdot (\sigma_\alpha \nabla u_h)$, and

$$\gamma_{11} = -(\sigma \partial_{x_1} u_h + \frac{\varepsilon}{z} u_h) \text{ if } x_1 = 0,$$

$$\gamma_{12} = -(\sigma \partial_{x_2} u_h + \frac{1}{z} u_h \text{ if}) \ x_2 = 0,$$

$$\gamma_{21} = -\sigma \partial_{x_1} u_h + \frac{\varepsilon}{z} u_h \text{ if } x_1 = 1,$$

$$\gamma_{22} = -\sigma \partial_{x_2} u_h + \frac{1}{z} u_h \text{ if } x_2 = 1.$$

Note also that the Dirichlet boundary condition (10) takes the form

$$u_h = 0 \text{ if } x_1 = 0, \tag{33}$$

$$u_h = -R_e I \text{ if } x_2 = 0, \tag{34}$$

$$u_h = 0 \text{ if } x_1 = 1, \tag{35}$$

$$u_h = R_e I \text{ if } x_2 = 1. \tag{36}$$

Following [19], we approximate the problem (28)–(32) with a second-order difference scheme as follows. On the closure $\overline{\Omega}$ we introduce a uniform grid

$$\overline{G} = \{x_{ij} = (x_1(i), x_2(j)) : x_1(i) = ih, x_2(j) = jh, hN = 1, i, j = 0, 1, ..., N\}.$$

Let y be a grid function defined on $\overline{G}$. Then the problem (28)–(32) is approximated by its difference analogue which is a system of linear equations

$$Ay = F, \tag{37}$$

where $F = F_h + (2/h)(\Gamma_1 + \Gamma_2)$, and the self-adjoint difference operator A has the form

$$A = A_1 + A_2,\ A_1 = A_2^{\star},$$

where

$$A_k y = \begin{cases} \frac{2}{h}(a_k^+ y_{x_k} - \psi y) & \text{if } x_k = 0, \\ (a_k y_{\bar{x}_k})_{x_k} & \text{if } h \le x_k \le 1-h, \\ \frac{2}{h}(-a_k y_{\bar{x}_k} - \psi y) & \text{if } x_k = 1, \end{cases} \tag{38}$$

$$\Gamma_k = \begin{cases} \gamma_{1k} & \text{if } x_k = 0, \\ 0 & \text{if } h \le x_k \le 1-h, \\ \gamma_{1k} & \text{if } x_k = 1, \end{cases} \tag{39}$$

$$\psi = \begin{cases} \frac{\varepsilon}{z} & \text{if } x_1 = 0 \text{ or } x_2 = 0, \\ \frac{1}{z} & \text{if } x_1 = 1 \text{ or } x_2 = 1. \end{cases} \tag{40}$$

The entries of the matrix A are given by

$$a_1 = \frac{1}{2}\left[\sigma_\alpha(x_1(i), x_2(j)) + \sigma_\alpha(x_1(i-1), x_2(j))\right],\ \ a_2 = \frac{1}{2}\left[\sigma_\alpha(x_1(i), x_2(j)) + \sigma_\alpha(x_1(i), x_2(j-1))\right],$$
$$a_1^+ = \frac{1}{2}\left[\sigma_\alpha(x_1(i+1), x_2(j)) + \sigma_\alpha(x_1(i), x_2(j))\right], a_1^+ = \frac{1}{2}\left[\sigma_\alpha(x_1(i), x_2(j+1)) + \sigma_\alpha(x_1(i), x_2(j))\right].$$

The corresponding derivatives are approximated by the finite differences

$$(a_1 y_{\bar{x}_1})_{x_1} = \frac{1}{h^2}\left(a_1(i+1, j)(y_{i+1,j} - y_{i,j}) - a_1(i, j)(y_{i,j} - y_{i-1,j})\right),$$
$$(a_2 y_{\bar{x}_2})_{x_2} = \frac{1}{h^2}\left(a_2(i+1, j)(y_{i+1,j} - y_{i,j}) - a_2(i, j)(y_{i,j} - y_{i-1,j})\right),$$
$$y_{x_1} = \frac{1}{h}(y_{i+1,j} - y_{i,j}),\ \ y_{x_2} = \frac{1}{h}(y_{i,j+1} - y_{i,j}),$$
$$y_{\bar{x}_1} = \frac{1}{h}(y_{i,j} - y_{i-1,j}),\ \ y_{\bar{x}_2} = \frac{1}{h}(y_{i,j} - y_{i,j-1}).$$

Although the system (37) is uniquely solvable, the matrix A is ill-conditioned. To solve (37) numerically, a preconditioned conjugate gradient method (see, e.g., [3]) may be used. However, in some situations, e.g., when the dimension N is sufficiently large and data a is perturbed, it is difficult to construct a preconditioner from the original matrix A that would ensure the appropriate accuracy of a numerical solution. As an alternative, the regularized Kranosel'sky successive approximations [25] may also be used. Being tested on several systems with the ill-conditioned matrices, both techniques have demonstrated the high rate of convergence and computational efficiency. The relative l_2 and l_∞ errors do not exceed 10^{-5}.

5. Computer simulations of coupled physics conductivity imaging

In this section we demonstrate both the numerical convergence and computational effectiveness of the proposed method by performing computer simulations of coupled physics conductivity imaging (see, e.g., [15]). The numerical convergence study is also motivated by the following. Although the convergence of regularized successive iterations is established in Theorem 2, the Lax-Richtmyer equivalency theorem that consistent numerical approximation, stability and convergence are equivalent does not take place for the nonlinear and ill-posed problems. Moreover, in practice the internal data a is corrupted by noise. Under these conditions, the convergence result established in Theorem 2 does not take place at the fixed noise level and in finite precision. Here, the numerical convergence is understood in the sense that there exists a natural number K_α, such that for the fixed noise level and sufficiently fine grid the regularized successive iterations are close enough to the true solution for $k \ge K_\alpha$. In computer simulations all computations are performed on the Dell Precision workstation T5400 running under IDL 6.2.

5.1. Data simulation

The model conductivity σ is simulated as follows. A real abdominal CT image of a human, which is shown in the left upper corner in Fig. 3, is embedded into the unit square $\overline{\Omega}$, so that the space between the image and sides of the square is supposed to be filled with a homogeneous conductive medium with $\sigma(x) = 1$. The actual Hounsfield units of the linear attenuation coefficient measurements are rescaled to the realistic range [1, 1.8] S/m of the electrical conductivity typical to the biological tissues. The conductivity bounds are set up as $\underline{\sigma} = 0.9$ S/m and $\overline{\sigma} = 2$ S/m. The electrodes injecting/ejecting the dc-currents into Ω are placed on the opposite sides of the square, so that the electrode supports are given by

$$e_- = \{(x_1, 0) : a \le x_1 \le b, 0 \le a < 0, 0 < b \le 1\}$$
$$e_+ = \{(x_1, 1) : a \le x_1 \le b, 0 \le a < 0, 0 < b \le 1\}.$$

The electrode aperture $b - a$ varies from 1 to few step sizes, and $-I_- = I_+ = 5 \cdot 10^{-3}$ A, $z = 8 \cdot 10^{-3}$ $\Omega \cdot m^2$.

Given the model conductivity σ and the parameters indicated above, the forward Robin model (1)–(2) is used to simulate the voltage potential u_s in Ω. As in [16] and [26], the standard Galerkin finite element method is utilized to solve numerically this forward problem. To provide a sufficiently small truncation error, the basis elements and mesh density are accurately chosen. We find that using the first-order element basis with the number of elements of order of tens of thousands, as well using preconditioners when solving the resulting system of linear equations, allows for a small relative error of order 10^{-5}. Once u_s is computed, the simulated interior data is calculated as $a_s = \sigma |u_s|$. Note that due to the roundoff and truncation errors, a_s is just an approximation of the model data $\sigma |\nabla u|$, where u is the solution of the forward problem (1)–(2). To simulate the measured interior data $\tilde{a}$, we exploit the model of the additive normally distributed noise

$$\tilde{a} = a_s + \delta \cdot \frac{R}{||R||_2}, \tag{41}$$

where δ is the prescribed level of error and $R = R(0, 1)$ is the normally distributed pseudo-random matrix with the zero mean and standard deviation 1.

5.2. Choice of the regularization parameter α

Suppose a certain approximation $\tilde{a}$ of a is obtained from measurements, so that

$$\|\tilde{a} - a\|_{L_2(\Omega)} < \delta.$$

It follows from the theory of regularization (see, e.g., [1]) that the pair $(\tilde{a}, \delta)$ is the minimal *a priori* information needed to construct a regularized solution of the coupled physics inverse conductivity problem. Since the coupled physics inverse conductivity problem is nonlinear and ill-posed, exploiting the residual principle (see, e.g., [1]) for choosing the regularization parameter α does not ensure obtaining approximations in a sufficiently small proximity to the model conductivity σ. In this paper we utilize *a priori* choice of the regularization parameter. According to [1] and based on (12) and (13), we choose a function $\alpha = \alpha(\delta) > 0$, such that

$$\lim_{\delta \to 0} \alpha(\delta) = 0 \text{ and } \lim_{\delta \to 0} \frac{\delta}{\alpha(\delta)} = 0. \tag{42}$$

For example, the functions

$$\alpha(\delta) = C\delta^p, \tag{43}$$

where $C = const > 0$, satisfy this condition for any $0 < p < 1$. Because of the continuous dependence of a minimizer u_α on the parameter α, one may choose $\alpha(\delta)$, so that

$$\|\tilde{a} - a_{\alpha(\delta)}\|_{L_2(\Omega)} \le \|\tilde{a} - a\|_{L_2(\Omega)} < \delta,$$

where $a_{\alpha(\delta)} = \sigma_{\alpha(\delta)} |\nabla u_\alpha|$, and the pair $(\sigma_{\alpha(\delta)}, u_\alpha)$ is a regularized solution to the inverse conductivity problem.

5.3. On the reconstruction

We use the method of regularized successive iterations described in the section 4 in order to recover a regularized (minimum residual) conductivity σ_α from the perturbed internal data $\tilde{a}$. The perturbations are due to the roundoff and truncation errors, as well as to the additive normally distributed noise. In the numerical experiments the level δ of perturbations varies from 10^{-5} to $5 \cdot 10^{-2}$. We observe that the values of p ranging from 7/16 to 10/16 provide almost the same accuracy of reconstruction. Therefore, in the numerical experiments we fix $p = 1/2$. When approximating the coefficients φ and h in the Robin condition, varying the parameter ε from $5 \cdot 10^{-5}$ to 10^{-3} does not significantly change the accuracy of reconstruction. Therefore, in the numerical experiments we use the fixed parameter $\varepsilon = 10^{-3}$. In simulations of the noisy data we use the data samples each of which contains up to 20 sampling units modeling measurements. Since we perform reconstruction for every sampling unit, a regularized conductivity is represented by the mean reconstructed conductivity. In assessing the quality of reconstruction we use not only a comparison of σ_α with the model conductivity σ, but also we compare σ_α with the results of reconstruction obtained by another method. As such, we choose the Alternating Split Bregman (ASB) algorithm developed in [11] for coupled physics conductivity imaging, because it is tolerant to critical points of the boundary voltage potentials that may arise in the Robin model. As pointed out in [13], this is needed to provide the uniqueness to the weighted least gradient Dirichlet problem, and the ASB algorithm exploits the relation between the weighted least gradient Dirichlet and dual problems via the Bregman distance. Note that the method of finding extrema

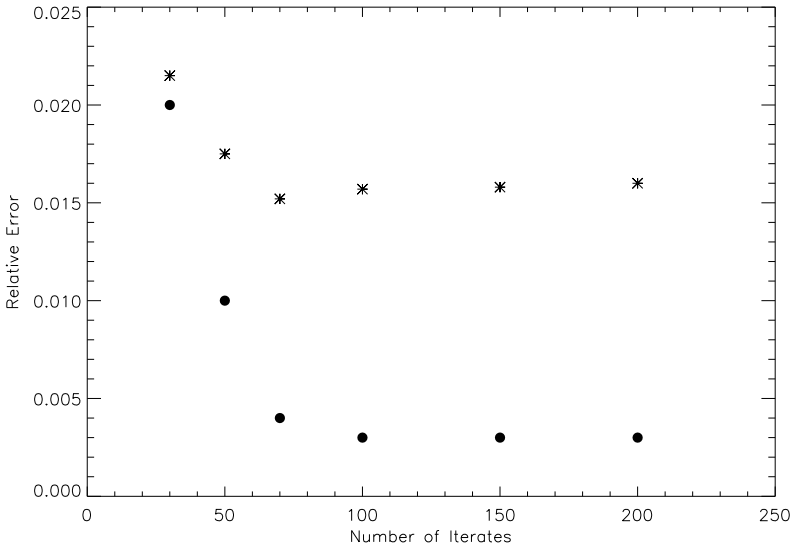

Fig. 1. Rates of numerical convergence for the ASB algorithm (asterisks) and method of regularized successive iterations (bullets) for the full electrode length.

of general convex functionals was originally proposed in convex optimization by Bregman [2] and later applied to image processing by Osher [18]. Since the ASB algorithm was developed for a weighted least gradient Dirichlet problem, we use the trace of u_s on the boundary $\partial\Omega$ as the Dirichlet condition in the ASB algorithm.

5.4. Some results of numerical experiments

In this section we demonstrate the computational effectiveness of the proposed method in the numerical experiments and compare its performance with the performance of the ASB algorithm.

5.4.1. The rate of numerical convergence and accuracy of reconstruction

The rate of numerical convergence and accuracy of reconstruction are two important quantitative characteristics of the computational effectiveness of a numerical method. To characterize the proposed method, we terminate the iterative process after 5, 10, 30, 50, 70, 100, 150, and 200 iterations, compute the mean reconstructed conductivities and calculate the relative l_2-errors versus the model conductivity (see its image in Fig. 3 at the left upper corner). In these experiments we set $|e_+| = |e_-| = 1$, i.e., the electrode length equals the side length of the unit square. In Fig. 1 we show the dependence of the relative l_2-error on the number of iterations. The results for the numbers 5 and 10 are omitted because of the large values of errors. As in [11] (see Figure 7), we observe that both methods exhibit almost the same rate of numerical convergence, whereas the accuracy of reconstruction provided by the method of regularized successive approximations is much better ($3 \cdot 10^{-3}$ vs. $1.5 \cdot 10^{-2}$)). This is also confirmed visually (see images in Fig. 3 in the middle of the upper row and at the right upper corner).

5.4.2. Effects of the electrode length

The other important characteristic is the sensitivity of a numerical method to variations of the electrode length. Although a medium is supposed to be conductive, the equipotential lines, being beginning and ending on the electrodes, span differently the domain Ω containing the inhomogeneities. The shrinking of the electrode length implies a redistribution of equipotential lines inside Ω, which is becoming more and more nonuniform as shrinking goes to be smaller and smaller. As a result of such an effect, the many-to-one boundary voltage potentials may arise. Apparently, this effect is particularly pronounced for the small electrode length and manifests itself in the appearance of some singularity points at the top of the images in the right corner of the lower row in Fig. 3. Therefore, one may expect that variations of the electrode length would influence the accuracy of the proposed method. To further investigate this effect, we perform reconstructions for the various electrode lengths ranging from few step sizes to the full electrode length. We have found that variations do not affect the rate of numerical convergence for both methods. As an example, in Fig. 2 we show the rates of convergence for the two step size electrode length. The variations of the electrode length affect slightly the accuracy of reconstruction, though the method of regularized successive approximations is more tolerant to such variations than the ASB algorithm.

5.4.3. Robustness

To further investigate robustness of the proposed method, i.e., its ability to cope with perturbations, we perform the numerical experiments with the statistically perturbed data $\tilde{a}$ which is simulated in accordance with (41). The regularized

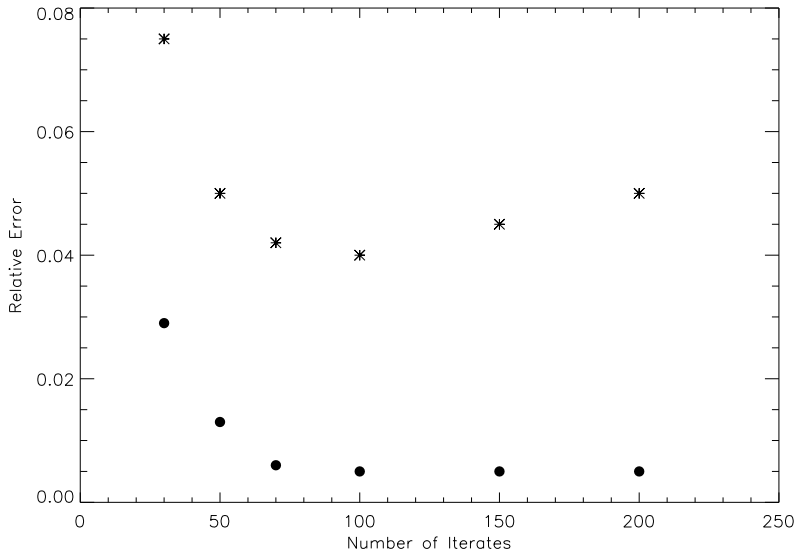

Fig. 2. Rates of numerical convergence for the ASB algorithm (asterisks) and method of regularized successive iterations (bullets) for the two step size electrode length.

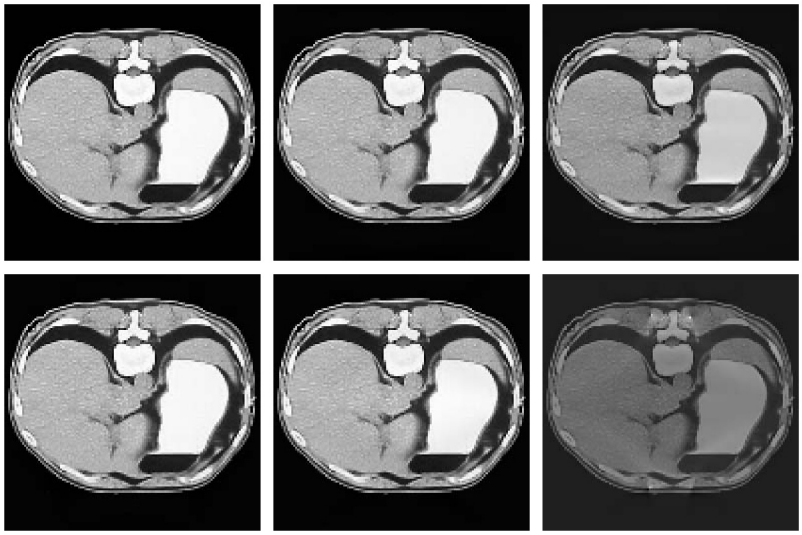

Fig. 3. Comparison of the mean reconstructed conductivities recovered from the noiseless internal data.

conductivity is recovered from the perturbed internal data $\tilde{a}$ with the noise level δ varying from 10^{-3} to $5 \cdot 10^{-2}$. The constant $1 < C < 10$ in the formula (43) is chosen by trials in order to provide the best accuracy. Correspondingly to the noise level, we set $C = 1.05, 1.2$, and 1.24. Fig. 4 demonstrates performance of the proposed method. In the upper row we show the mean reconstructed conductivities for the full electrode length and the noise level 10^{-3}, 10^{-2}, and $5 \cdot 10^{-2}$ (from left to right). The corresponding relative l_2-errors of reconstruction are $4.5 \cdot 10^{-3}$, $7.9 \cdot 10^{-3}$, and $4.3 \cdot 10^{-2}$. In the lower row we show the mean reconstructed conductivities recovered for the electrode length of $1/2, 1/4$, and two step sizes (from left to right)) with the fixed noise level 10^{-2}. The corresponding relative l_2-errors of reconstruction are $1.1 \cdot 10^{-2}$, $1.8 \cdot 10^{-2}$, and $5.3 \cdot 10^{-2}$.

6. Concluding remarks

In this paper we have proposed and developed the method of regularized successive approximations for the numerical solution of an inverse conductivity problem arising in coupled physics conductivity imaging. The new method is based on a regularized weighted least gradient Robin problem. It follows from the analysis of this problem that some good approximations of conductivity can be approximately recovered from the magnitude of one internal current density field without knowledge of the boundary voltage potential. We have developed the computationally efficient iterative procedure

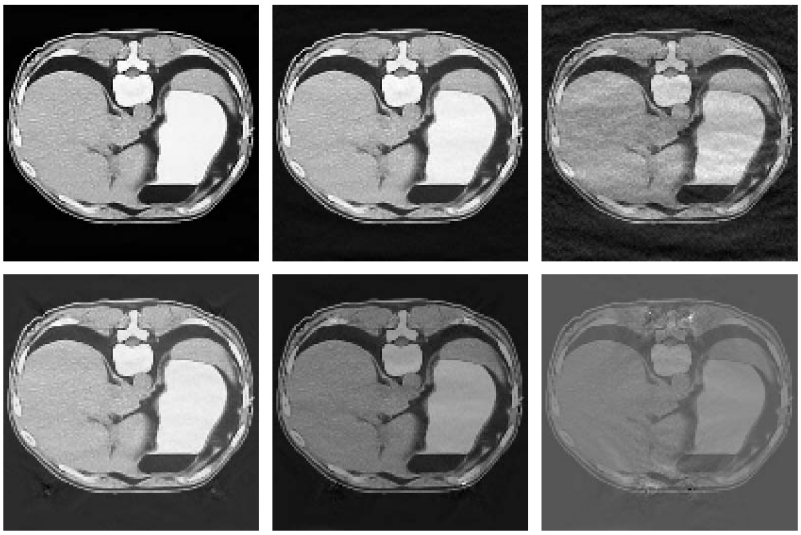

Fig. 4. Comparison of the means reconstructed conductivities recovered from the noisy interior data.

for constructing the minimizing sequences for the regularized weighted least gradient functional. This procedure consists of successive numerical solutions of the approximate Robin problems. We have performed the numerical convergence study and demonstrated that the proposed method, being sufficiently fast and robust, allows for the appropriate accuracy of regularized solutions even for the small electrode lengths. The results of some numerical experiments give rise to the idea that exploiting the concept of the variable regularization parameter may improve the rate of numerical convergence and accuracy of reconstruction. We reserve investigating this issue for further work.

Acknowledgement

The work of A. Tamasan has been supported by the NSF grant DMS-1907097. The work of A. Timonov has been supported by the NSF grant DMS-1818882.

References

[1] A. Bakushinsky, A. Goncharsky, Ill-Posed Problems: Theory and Applications, Springer, New York, 1999.
[2] L. Bregman, The relaxation method of finding the common points of convex sets and its application to the solution of problems of convex optimization, USSR Comput. Math. Math. Phys. 7 (1967) 200–217.
[3] G.H. Golub, C.F. Van Loan, Matrix Computations, 3rd ed., The Johns Hopkins University Press, 1996.
[4] R.L. Jerrard, A. Moradifam, A.I. Nachman, Existence and uniqueness of minimizers of general least gradient problems, J. Reine Angew. Math. 734 (2018) 71–97.
[5] S. Kim, O. Kwon, J.K. Seo, J.R. Yoon, On a nonlinear partial differential equation arising in magnetic resonance electrical impedance tomography, SIAM J. Math. Anal. 34 (2002) 511–526.
[6] O. Kwon, J.Y. Lee, J.R. Yoon, Equipotential line method for magnetic resonance electrical impedance tomography, Inverse Probl. 18 (2002) 1089–01100.
[7] C. Montalto, P.I. Stefanov, Stability of coupled physics inverse problems with one internal measurement, Inverse Probl. 29 (2013) 125004.
[8] C. Montalto, A. Tamasan, Stability in conductivity imaging from partial measurements of one interior current, Inverse Probl. Imaging 11 (2017) 339–353.
[9] A. Moradifam, A. Nachman, A. Tamasan, Conductivity imaging from one interior measurement in the presence of perfectly conducting and insulating inclusions, SIAM J. Math. Anal. 44 (2012) 3669–3690.
[10] A. Moradifam, A. Nachman, A. Tamasan, Uniqueness of minimizers of weighted least gradient problems arising in conductivity imaging, Calc. Var. Partial Differ. Equ. 57 (2018) 6–27.
[11] A. Moradifam, A. Nachman, A. Timonov, A convergent algorithm for the hybrid problem of reconstructing conductivity from minimal interior data, Inverse Probl. 28 (2012) 084003.
[12] A. Nachman, A. Tamasan, A. Timonov, Conductivity imaging with a single measurement of boundary and interior data, Inverse Probl. 23 (2007) 2551–2563.
[13] A. Nachman, A. Tamasan, A. Timonov, Recovering the conductivity from a single measurement of interior data, Inverse Probl. 25 (2009) 035014.
[14] A. Nachman, A. Tamasan, A. Timonov, Reconstruction of planar conductivities in subdomains from incomplete data, SIAM J. Appl. Math. 70 (2010) 3342–3362.
[15] A. Nachman, A. Tamasan, A. Timonov, Current density impedance imaging, Contemp. Math.- Am. Math. Soc. 559 (2011) 1335–1351.
[16] A. Nachman, A. Tamasan, J. Veras, A weighted minimum gradient problem with complete electrode model boundary conditions for conductivity imaging, SIAM J. Appl. Math. 76 (2016) 1321–1343.
[17] Z. Nashed, A. Tamasan, Structural stability in a minimization problem and applications to conductivity imaging, Inverse Probl. Imaging 5 (2010) 219–236.
[18] S. Osher, et al., An iterative regularization method for total variation-based image restoration, Multiscale Model. Simul. 4 (2005) 460–489.
[19] A.A. Samarskii, Theory of Difference Schemes, Marcell Decker Inc., New York, 2001.
[20] D.C. Scott, M.L. Joy, R.L. Armstrong, et al., Measurement of nonuniform current density by magnetic resonance, IEEE Trans. Med. Imaging 10 (1991) 362–374.

[21] E. Somersalo, M. Cheney, D. Isaacson, Existence and uniqueness for electrode models for electric current computed tomography, SIAM J. Appl. Math. 54 (1992) 1023–1040.
[22] A. Tamasan, A. Timonov, Coupled physics electrical conductivity imaging, Eurasian J. Math. Comput. Appl. 2 (2014) 5–29.
[23] A. Tamasan, A. Timonov, A regularized weighted least gradient problems for conductivity imaging, Inverse Probl. 35 (2019) 045006.
[24] A. Tamasan, A. Timonov, J. Veras, Stable reconstruction of regular 1-harmonic maps with a given trace at the boundary, Appl. Anal. 94 (6) (2015), https://doi.org/10.1080/00036811.2014.918260.
[25] A. Timonov, Factorised preconditionings of successive approximations in finite precision, BIT Numer. Math. 41 (2001) 582–598.
[26] P. Vauhkonen, M. Vauhknoen, T. Savolainen, et al., Three-dimensional electrical impedance tomography based on the complete electrode model, IEEE Trans. Biomed. Eng. 46 (1999) 1150–1160.
[27] W.P. Ziemer, Weakly Differentiable Functions, Springer, New York, 1969.